Disentangling the triadic interactions in Navier-Stokes equations*

Ganapati Sahoo[1] and Luca Biferale[1]

[1]*Department of Physics & INFN, University of Rome Tor Vergata, Via della Ricerca Scientifica 1, 00133 Rome, Italy.*

(Dated: November 2, 2015)

We study the role of helicity in the dynamics of energy transfer in a modified version of the Navier-Stokes equations with explicit breaking of the mirror symmetry. We select different set of triads participating in the dynamics on the basis of their helicity content. In particular, we remove the negative helically polarized Fourier modes at all wavenumbers except for those falling on a localized shell of wavenumber, $|\boldsymbol{k}| \sim k_m$. Changing k_m to be above or below the forcing scale, k_f, we are able to assess the energy transfer of triads belonging to different interaction classes. We observe that when the negative helical modes are present only at wavenumber smaller than the forced wavenumbers, an inverse energy cascade develops with an accumulation of energy on a stationary helical condensate. Vice versa, when negative helical modes are present only at wavenumber larger than the forced wavenumbers, a transition from backward to forward energy transfer is observed in the regime when the minority modes become energetic enough.

INTRODUCTION

It is known that the energy in a three dimensional homogeneous and isotropic turbulent flow cascades forward, from the forcing scales to the dissipative scales [1]. When Reynolds number is high enough, an intermediate range of scales develops where the energy flux is constant [2]. However, systems like rotating flows [3, 4], flows confined along one direction [5] and flows of conducting materials [6] show an inverse energy transfer toward larger and larger scales. As a result, it is still not clear what are the internal dynamical mechanisms that trigger the direction of the energy flux in fully developed turbulence. In this paper, we present a series of numerical experiments done on a modified version of the three-dimensional Navier-Stokes equations where a subset of Fourier modes have been removed. There are many different ways to achieve a mode reduction, from the usual Galerkin truncation of all modes with $|\boldsymbol{k}| > k_{\max}$ to more refined self-similar truncation done on a fractal-Fourier set [7]. Here, we are interested to further explore the possibility to reduce mode on the basis of their helicity content [8–10]. Helicity, together with energy, is an inviscid invariant of three-dimensional Navier-Stokes equation and it is known to play a key role both for hydrodynamical and magnetohydrodynamical systems [11–24]. In previous works [10, 25] we have shown that by constraining the velocity field to develop fluctuations with only one sign of helicity, the energy flows backward: from the forced scale to the largest scale in the system, without reaching a steady state if not confined on a finite box or without the addition of external friction. More recently, we have shown that the inverse cascade regime, observed for the fully helical case, is highly fragile [26]: it is enough to have a tiny number of helical modes with the opposite sign distributed uniformly on the Fourier space to revert the system to a forward cascade regime. Such a conclusion is also supported by arguments based on absolute equilibrium [27, 28]. In this paper we explore the case when all Fourier modes have the same helicity (say positive) except for a small subset possessing also the opposite (negative) helicity. The latter being limited to belong to a tiny shell in Fourier space. The goal is to make a further step toward a better understanding of the dynamics of energy transfer in Navier-Stokes equations, triad-by-triad. The paper is organized as follows: In Sec. 2 we briefly describe helical decimation and write the Navier-Stokes equations for helical Fourier modes; In Sec. 3 we discuss the results from our direct numerical simulations for two different series of computations, either when the negative helical modes are confined to a shell of wavenumbers larger than the force scale or in the opposite case. Conclusions can be found in Sec. 4.

HELICALLY DECOMPOSED NAVIER-STOKES EQUATIONS

The velocity field in a periodic domain is expressed by the Fourier series

$$\boldsymbol{u}(\boldsymbol{x}) = \sum_{\boldsymbol{k}} \hat{\boldsymbol{u}}_{\boldsymbol{k}} e^{i\boldsymbol{k}\cdot\boldsymbol{x}}, \tag{1}$$

where the modes $\hat{\boldsymbol{u}}_{\boldsymbol{k}}$ satisfy the incompressibility condition $\boldsymbol{k}\cdot\hat{\boldsymbol{u}}_{\boldsymbol{k}} = 0$ and can be exactly decomposed in terms of the helically polarized waves as [8, 9]

$$\hat{\boldsymbol{u}}_{\boldsymbol{k}} = u^+_{\boldsymbol{k}}\boldsymbol{h}^+_{\boldsymbol{k}} + u^-_{\boldsymbol{k}}\boldsymbol{h}^-_{\boldsymbol{k}}. \tag{2}$$

The eigenvectors of the curl $\boldsymbol{h}^\pm_{\boldsymbol{k}}$ are given by

$$\boldsymbol{h}^\pm_{\boldsymbol{k}} = \hat{\nu}_{\boldsymbol{k}} \times \hat{k} \pm i\hat{\nu}_{\boldsymbol{k}}, \tag{3}$$

*Postprint version of the manuscript published in Eur. Phys. J. E **38**, 114 (2015)

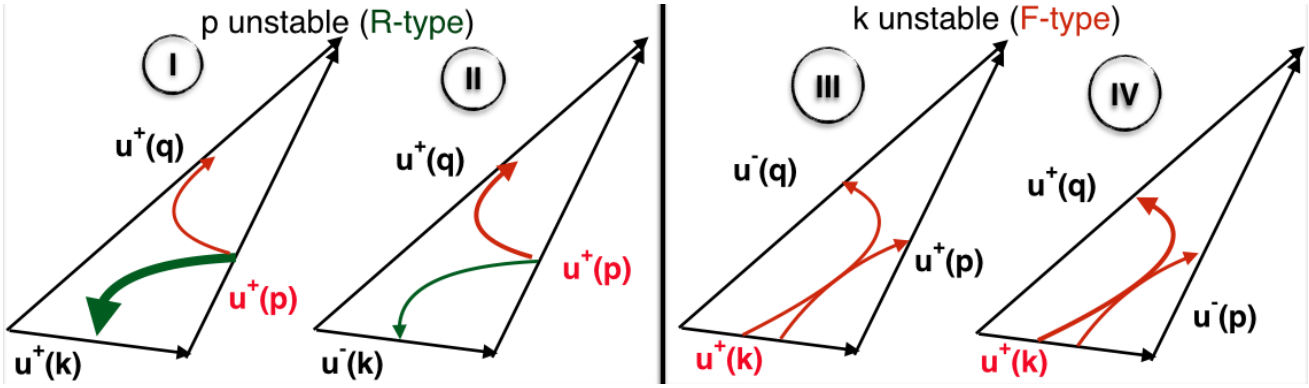

FIG. 1: (Color online) Schematic presentation of triads [8]: Triads where the two largest wavenumbers have the same sign of helicity are responsible for a reverse transfer of energy and are called of R-type. They include triads of Class I and of Class II. Triads where the two largest wavenumbers have opposite sign of helicity are responsible for forward transfer of energy and are called of F-type. They include triads in Class III and Class IV. For R-type (F-type) the Fourier mode with the medium (smallest) wavenumber is unstable and transfers energy to the other two Fourier modes. The arrows (green for reverse and red for forward) show direction of energy transfer.

so that $i\boldsymbol{k}\times\boldsymbol{h}_{\boldsymbol{k}}^{\pm}=\pm k\boldsymbol{h}_{\boldsymbol{k}}^{\pm}$; where $\hat{\nu}_{\boldsymbol{k}}$ is an unit vector orthogonal to $\boldsymbol{k}$ such that $\hat{\nu}_{\boldsymbol{k}}=-\hat{\nu}_{-\boldsymbol{k}}$ to enforce reality of the field. One can choose for example [8]:

$$\hat{\nu}_{\boldsymbol{k}}=\frac{\boldsymbol{z}\times\boldsymbol{k}}{||\boldsymbol{z}\times\boldsymbol{k}||}, \tag{4}$$

where $\boldsymbol{z}$ is any arbitrary vector. The eigenvectors $\boldsymbol{h}_{\boldsymbol{k}}^{\pm}$ satisfy the orthogonality condition $\boldsymbol{h}_{\boldsymbol{k}}^{s}\cdot\boldsymbol{h}_{\boldsymbol{k}}^{t*}=2\delta_{st}$, where $s,t=\pm$ denote the signs of the helicity and $*$ is for the complex conjugate. We define a projector

$$\mathcal{P}_{\boldsymbol{k}}^{\pm}\equiv\frac{\boldsymbol{h}_{\boldsymbol{k}}^{\pm}\otimes\boldsymbol{h}_{\boldsymbol{k}}^{\pm*}}{\boldsymbol{h}_{\boldsymbol{k}}^{\pm*}\cdot\boldsymbol{h}_{\boldsymbol{k}}^{\pm}}, \tag{5}$$

which projects the Fourier modes of the velocity on eigenvectors $\boldsymbol{h}_{\boldsymbol{k}}^{\pm}$ as

$$\mathcal{P}_{\boldsymbol{k}}^{\pm}\hat{\boldsymbol{u}}_{\boldsymbol{k}}=\hat{\boldsymbol{u}}_{\boldsymbol{k}}^{\pm}=u_{\boldsymbol{k}}^{\pm}\boldsymbol{h}_{\boldsymbol{k}}^{\pm}. \tag{6}$$

The Navier-Stokes equations can be decomposed in terms of the evolution of velocities with positive or negative sign of helicity as follows:

$$\frac{\partial\boldsymbol{u}^{\pm}(\boldsymbol{x})}{\partial t}+\mathcal{D}^{\pm}\mathbf{N}[\boldsymbol{u}(\boldsymbol{x}),\boldsymbol{u}(\boldsymbol{x})]=\nu\nabla^{2}\boldsymbol{u}^{\pm}(\boldsymbol{x})+\mathbf{f}^{\pm}, \tag{7}$$

where the operator $\mathcal{D}^{\pm}(\boldsymbol{u})$ acts on a generic three-dimensional vector field by projecting all Fourier components on $\boldsymbol{h}_{\boldsymbol{k}}^{\pm}$:

$$\mathcal{D}^{\pm}\boldsymbol{u}(\boldsymbol{x})\equiv\sum_{\boldsymbol{k}}e^{i\boldsymbol{k}\cdot\boldsymbol{x}}\,\mathcal{P}_{\boldsymbol{k}}^{\pm}\hat{\boldsymbol{u}}_{\boldsymbol{k}}, \tag{8}$$

and $\mathbf{N}[\boldsymbol{u}(\boldsymbol{x}),\boldsymbol{u}(\boldsymbol{x})]$ is the nonlinear terms of the Navier-Stokes equations [25]. The total energy and the total helicity can also be easily expressed in terms of the helical modes:

$$E=\int d^{3}x\,|\boldsymbol{u}(\boldsymbol{x})|^{2}=\sum_{\boldsymbol{k}}|u_{\boldsymbol{k}}^{+}|^{2}+|u_{\boldsymbol{k}}^{-}|^{2}, \tag{9}$$

$$H=\int d^{3}x\,\boldsymbol{u}(\boldsymbol{x})\cdot\boldsymbol{\omega}(\boldsymbol{x})=\sum_{\boldsymbol{k}}k(|u_{\boldsymbol{k}}^{+}|^{2}-|u_{\boldsymbol{k}}^{-}|^{2}), \tag{10}$$

where $\boldsymbol{\omega}(\boldsymbol{x})=\nabla\times\boldsymbol{u}(\boldsymbol{x})$ is the vorticity. From the above expression one can introduce the energy spectrum for positive and for negative helical modes [19, 20]:

$$E^{+}(k)=\sum_{|\boldsymbol{k}|\in[k,k+1]}|u_{\boldsymbol{k}}^{+}|^{2}; \tag{11}$$

$$E^{-}(k)=\sum_{|\boldsymbol{k}|\in[k,k+1]}|u_{\boldsymbol{k}}^{-}|^{2}. \tag{12}$$

Plugging the decomposition (2) in to the Navier-Stokes equations (7) it is easy to realize that the nonlinear term consists of triadic interactions with eight (four for the evolution of u^{+} and four for the evolution of u^{-}) possible helical combinations of the generic modes $u_{\boldsymbol{k}}^{s_{\boldsymbol{k}}}$, $u_{\boldsymbol{p}}^{s_{\boldsymbol{p}}}$, $u_{\boldsymbol{q}}^{s_{\boldsymbol{q}}}$ forming an interacting triad, i.e., $\boldsymbol{k}+\boldsymbol{p}+\boldsymbol{q}=0$, for $s_{\boldsymbol{k}}=\pm$, $s_{\boldsymbol{p}}=\pm$, $s_{\boldsymbol{q}}=\pm$ [8] (see fig. 1 where for simplicity we assume that $k\leq p\leq q$). The four classes of triads are classified as follows: Class I, containing triads formed with all wavenumbers having the same sign of helicity, i.e., $(+,+,+)$; Class II, made of triads where the two smallest wavenumbers have opposite sign of helicity and the two largest wavenumbers have the same sign of helicity, i.e., $(-,+,+)$; Class III, containing triads where the two smallest wavenumbers have the same sign of helicity and the two largest wavenumbers have an opposite sign of helicity, i.e., $(+,+,-)$; and Class IV, made of triads where the two smallest wavenumbers and the two largest wavenumbers have opposite sign of helicity, i.e., $(+,-,+)$ (see fig. 1). In [8], studying the instability of the energy

exchange among modes of each single triad, it was argued that the triads in Class III and Class IV transfer energy from the smallest wavenumber to the other two wavenumbers and are responsible for the forward cascade of energy. Whereas for the triads in Class I and Class II, the Fourier mode with the medium wavenumber transfers energy to the other two Fourier modes. These sets of triads might then contribute to both forward and backward energy transfers. The presence of competing interactions might suggest that the direction of the energy transfer mechanism is not set *a priori*. Depending on the empirical realization (the forcing scheme, the boundary conditions, the coupling with other active dynamical fields as for the case of conducting flows [5, 6, 29, 30]) different directions of the energy could be developed. As said, in the whole system where all triads are present and with a neutral homogeneous and isotropic external forcing, energy is observed to be transferred forward: from large to small scales. On the other hand, a system in which only modes of one sign of helicity are present, i.e., the dynamics is restricted to interacting triads with $s_{\boldsymbol{k}} = s_{\boldsymbol{p}} = s_{\boldsymbol{q}}$ (Class I), energy cascades from small scales to the large scales [25]. This was reconducted to the fact that helicity becomes a sign-definite quantity for such subset of interactions. In a recent work it was observed [26] that presence of few percent of modes with opposite sign of helicity changes the direction of energy transfer in a singular manner: a few modes with both sign of helicity at all scales, even though one type is a small fraction of other type, allows formation of triads with two largest wavenumbers having opposite signs of helicity which efficiently transfers energy to the small scales.

In this work we attempt to control the energy transfer mechanism in presence of two different set of triads (Class II and Class IV). To do that we remove the negative helical modes for all wavenumbers, except for those falling in one shell of Fourier modes $|\boldsymbol{k}| \in D_m$ with $D_m \equiv \{\boldsymbol{k} : |\boldsymbol{k}| \in [k_m, k_m + 1]\}$. We consider two cases (i) $k_m < k_f$ and (ii) $k_m > k_f$, where k_f is the typical wavenumber where we apply the external forcing mechanism. To do that we define an operator $\mathcal{D}_m$ which projects the velocity on $\boldsymbol{h}^+_{\boldsymbol{k}}$ for wavenumbers outside the coset of D_m:

$$\boldsymbol{u}'(\boldsymbol{x}) \equiv \mathcal{D}_m \boldsymbol{u}(\boldsymbol{x}) \equiv \sum_{\boldsymbol{k}} e^{i\boldsymbol{k}\boldsymbol{x}} \left[(1 - \gamma_{\boldsymbol{k}}) + \gamma_{\boldsymbol{k}} \mathcal{P}^+_{\boldsymbol{k}}\right] \hat{\boldsymbol{u}}_{\boldsymbol{k}}, \quad (13)$$

where $\gamma_{\boldsymbol{k}} = 0$ for $\boldsymbol{k} \in D_m$ and $\gamma_{\boldsymbol{k}} = 1$ otherwise. The decimated three-dimensional Navier-Stokes equations are given by:

$$\partial_t \boldsymbol{u}' = \mathcal{D}_m[-(\boldsymbol{u}' \cdot \nabla)\boldsymbol{u}' - \boldsymbol{\nabla} p'] + \nu \Delta \boldsymbol{u}' + \mathbf{f}', \quad (14)$$

where p' is the pressure, ν is the viscosity and $\mathbf{f}'$ is the external forcing (see later for details). Although nonlinear terms of the decimated Navier-Stokes equations do not have Lagrangian properties [31], it can still be shown

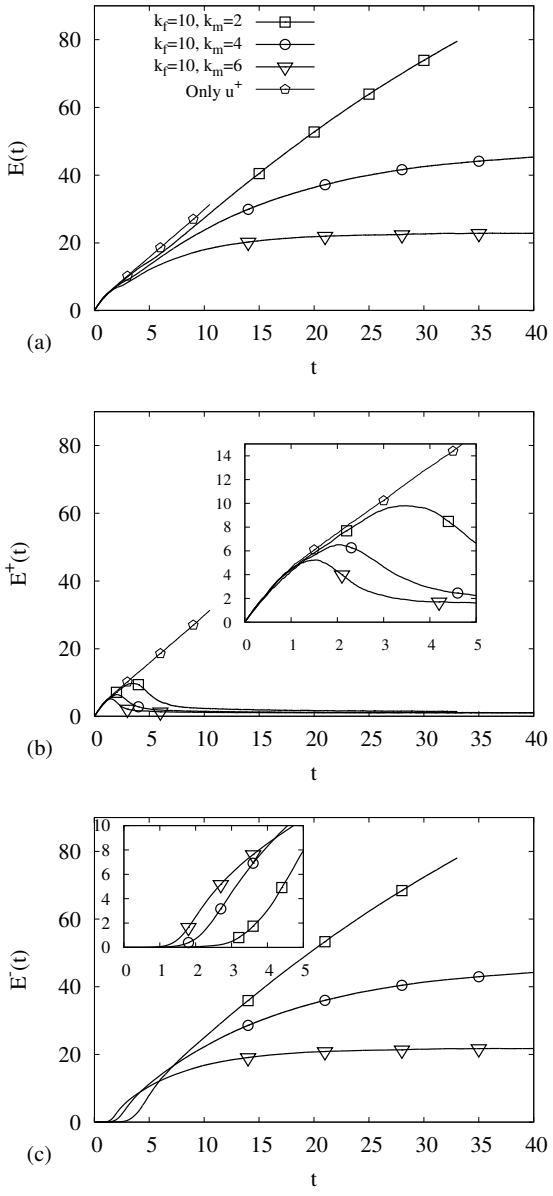

FIG. 2: Time evolution of the energy based on (a) all modes, (b) only positive helical modes, and (c) only negative helical modes, for the three cases where $k_f \in [10, 12]$ and $u^-_{\boldsymbol{k}} = 0$ except wavenumbers around $k_m = 2, 4, 6$. In the insets of panel (b) and (c) we show an enlargement of the initial period. Notice that the dynamics is first dominated by the sucking of energy by the positive helical modes at low wavenumbers and then it switches to transfer energy only to the negative ones. In panels (a) and (b) we also show the results for the growth of energy when only positive helical modes are present. In the latter case the growth of the energy in the positive helical modes is not stopped.

that both energy

$$E = \sum_{\boldsymbol{k}} (|u^+_{\boldsymbol{k}}|^2 + (1 - \gamma_{\boldsymbol{k}})|u^-_{\boldsymbol{k}}|^2), \quad (15)$$

RUN	N	L	k_f	k_m	ν	δt	F_0
R1	512	2π	$[10, 12]$	6	0.002	0.0001	5
R2	512	2π	$[10, 12]$	4	0.002	0.0001	5
R3	512	2π	$[10, 12]$	2	0.002	0.0001	5
R4	512	2π	$[4, 6]$	10	0.001	0.0001	5
R5	512	2π	$[4, 6]$	16	0.001	0.0001	5

TABLE I: N: number of collocation points along each axis. L: size of the simulation box. k_f: range of forced wavenumbers. k_m: wavenumber of the shell with also negative helical modes. ν: kinematic viscosity. δt: time step. F_0: forcing amplitude.

and helicity

$$H = \sum_{\boldsymbol{k}} k(|u^+_{\boldsymbol{k}}|^2 - (1-\gamma_{\boldsymbol{k}})|u^-_{\boldsymbol{k}}|^2), \tag{16}$$

are invariants of eq.(14) in the inviscid and unforced limit.

DIRECT NUMERICAL SIMULATIONS

A pseudo-spectral spatial method is adopted to solve eqs. (14), fully dealiased with the two-thirds rule; time stepping is implemented with a second-order Adams-Bashforth scheme. We performed different run up to a resolution of 512^3 collocation points, by changing the forced wavenumbers and the shell of modes where negative helical waves are retained. We applied a random Gaussian force with

$$\langle f_i(\boldsymbol{k}, t) f_j(\boldsymbol{q}, t')\rangle = F(k)\delta(\boldsymbol{k}-\boldsymbol{q})\delta(t-t')Q_{ij}(\boldsymbol{k}),$$

where the projector $Q_{ij}(\boldsymbol{k})$ ensures incompressibility and $F(k) = F_0 k^{-3}$; the forcing amplitude F_0 is nonzero only for $k_f \in [k_{\min} : k_{\max}]$. Table. I lists the details of various simulations. Moreover, we always projected the forcing on its positive helical components in order to ensure maximal helicity injection. We carried out two sets of simulations; First we retained the negative helical modes in a shell of wavenumbers $\sim k_m$ smaller than the forced wavenumbers k_f, while in the second case we retained the negative helical modes at a $k_m > k_f$. In the first set, negative helical modes exist only at wavenumbers smaller than the forcing mechanisms so effectively we add triads of Class II to the triads of Class I. In the second set, negative helical modes exist at higher wavenumbers, resulting in the addition mainly of triads of Class III and Class IV.

Energy transfer for $k_m < k_f$

In this set of simulations we keep $k_f \in [10, 12]$ and change the value of k_m to 2, 4 and 6. Figure 2(a) shows the evolution of energy in the three cases. We always observe a steady inverse energy cascade which reaches a statistically steady state, except for $k_m = 2$ where the run was not long enough to stabilize the system. Notice that we never introduced an external energy sink at large scales. Therefore, a statistically stable system means that a stable large scale helical condensate is formed with an energy large enough to be dissipated directly by molecular viscosity. The growth of energy in the positive and negative helical modes are shown separately in fig. 2 (b) and (c). It is striking to note that in the steady state the negative helical modes, existing only at $k = k_m$, carry almost all the energy of the system, signaling that the inverse energy cascade process is very efficient to move energy to the opposite helical modes via Class II interactions. Moreover, the negative helical modes act as sinks and do not allow the inverse cascade to proceed further to larger scales, stabilizing a condensate to a given wavenumber, independent of the size of the box. A statistically stationary state is then reached only when molecular drag becomes efficient at such scales. Initially the growth of energy is in the positive helical modes, shown in the insets of panels (b) and (c). There is a critical change in the dynamics of the system when the negative helical modes become energetic enough (i.e., for the $k_m = 2$ case around $t \sim 3$). The positive helical modes at $k < k_m$ lose their energy as they form triads of Class III or Class IV with the negative helical modes and therefore contribute to the formation of condensate at $k \sim k_m$. To better understand the dynamics among different wavenumbers we show the spectrum of energy at different times in fig. 3, for the case $k_m = 2$. From fig. 3(a) we see that at initial times ($t < 2.0$) the growth of energy in the large scales ($k < k_f$) is due to an inverse transfer to the positive helical modes. This transfer is driven by triads of Class I. When the negative helical modes at $k = k_m$ becomes energetic enough ($t \sim 5$) the positive helical modes start to be depleted, leading for later times ($t \sim 9$) to a configuration where all the energy is concentrated only on the u^-_k, albeit they correspond to a small minority of the total number of degrees-of-freedom. Figure 3(c) shows the flux of total energy as a function of time. We observe a persistent constant positive flux corresponding to inverse cascade of energy in the range $k \in [k_m, k_f]$. This confirms that also triads of Class II lead to a reverse energy cascade. The energy is then directly dissipated by the viscous effect which becomes substantial for the highly energetic negative helical modes. This is shown in fig. 3(d), where we compare the energy flux due to the nonlinear terms,

$$\Pi_E(k) = \sum_{|\boldsymbol{k}'|<k} \hat{\boldsymbol{u}}^*_{\boldsymbol{k}'} \cdot \hat{\mathbf{N}}_{\boldsymbol{k}'}, \tag{17}$$

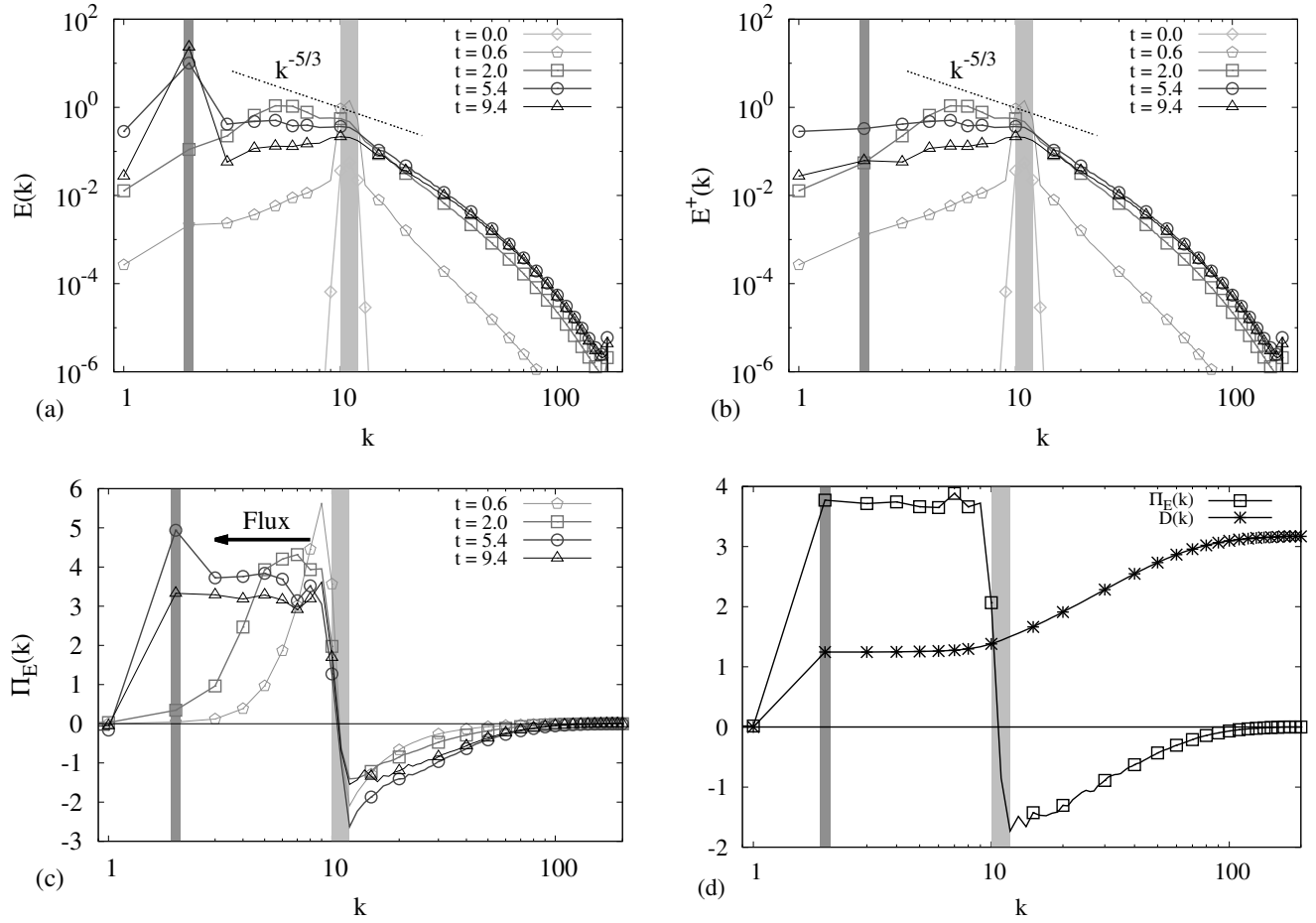

FIG. 3: (a) Log-log plot of total energy spectra at different times. (b) The same of (a) for the positive helical modes spectrum. The mismatch between the two spectra for $k = k_m$ is due to the energy of the negative helical modes. We have drawn a dashed line with slope of -5/3 to highlight the possible growth of inverse cascade spectrum when there is a large inertial range of scales. (c) Fluxes of energy (see definition (17)). (d) Comparision of energy flux $\Pi_{\rm E}(k)$ and dissipation $\mathrm{D}(k)$ (see text) at the time when the simulation is stopped ($t \sim 32$, see fig. 2). The forced wavenumbers at $k_f \in [10, 12]$ are marked with a light grey band, while the wavenumbers with negative helical modes around $k_m = 2$ are in dark grey.

across a wavenumber k, where

$$\hat{\mathbf{N}}_{\boldsymbol{k}} = \left(\mathbb{I} - \frac{\boldsymbol{k}\boldsymbol{k}}{k^2}\right)\left[\sum_{\boldsymbol{p}+\boldsymbol{q}=-\boldsymbol{k}} (\hat{\boldsymbol{u}}_{\boldsymbol{p}} \cdot \boldsymbol{q})\hat{\boldsymbol{u}}_{\boldsymbol{q}}\right] \tag{18}$$

is the nonlinear term in the Fourier space, and the total molecular dissipation in the same Fourier interval:

$$\mathrm{D}(k) = 2\nu \sum_{|\boldsymbol{k}'|<k} k'^2 E(k'). \tag{19}$$

It should be noted that with this definition (17) of energy flux, which has the opposite sign of what is commonly used, a positive/negative flux means the presence of an inverse/direct energy cascade. Let us stress that the viscous contribution does not match exactly the nonlinear transfer because the energy is still growing in time. Simulations for the case where $k_f = 4, 6$ reach a steady state earlier and they show a much better matching between the two contributions, see below panel (d) of fig. 4. Let us also notice that a sort of $k^{-5/3}$ scaling is observed in the inverse cascade regime as for the case when only Class I triads are present [25], at least up to the time when the condensate does not become too energetic to spoil the scaling properties.

In fig. 4 we show the results from the case where $k_m = 6$. The main interest to select this window is that in this way we can change the degree of nonlocality of the triad geometry. In [8] it was argued that in the scaling regime triads of Class II should display either a forward or a reverse energy transfer depending whether the ration between the smallest and the medium wavenumber $v = k/p$ is larger or smaller than 0.278. If we assume that the main energy transfer happens via a triad where two wavenumbers fall in the forced range and the other belong to the negative helical modes then we have $v = 0.6$

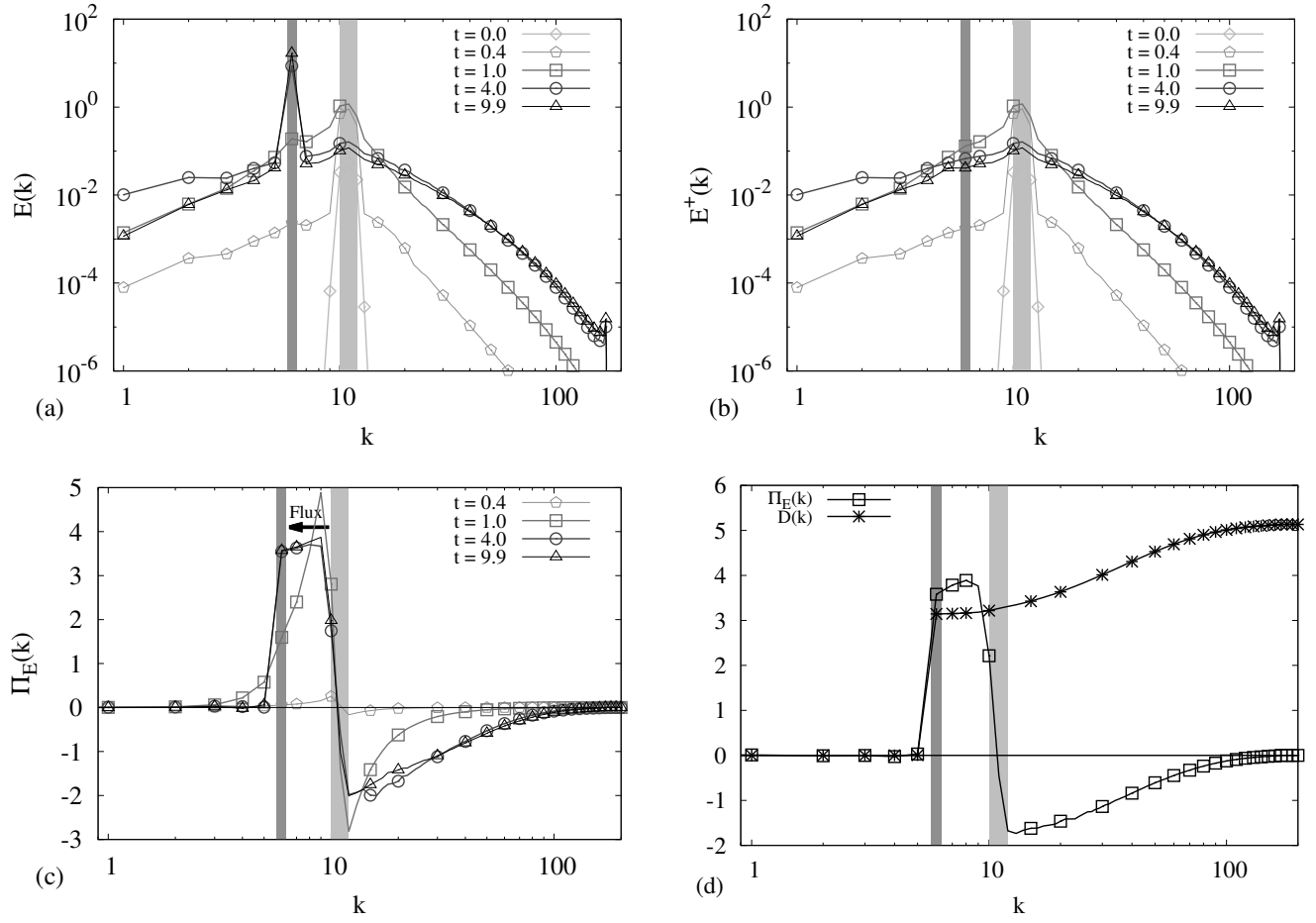

FIG. 4: The same of fig. 3 but for the case when $k_m = 6$, except for (d) where energy flux and dissipation are compared at $t \sim 40$ when the simulation is stopped (see fig. 2).

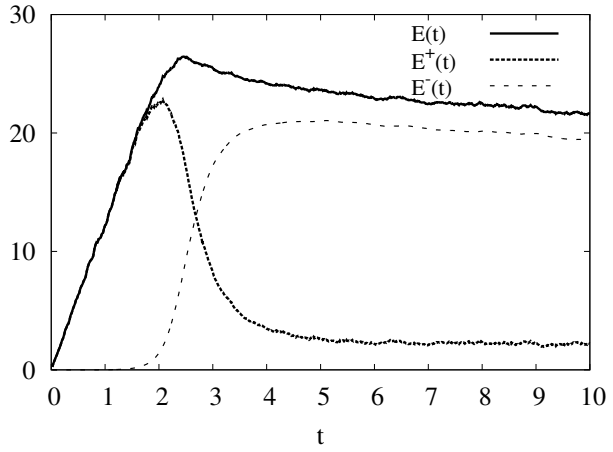

FIG. 5: Time evolution of total energy $E(t)$, energy of positive helical modes $E^+(t)$, and energy of negative helical modes $E^-(t)$ when $k_f \in [4, 6]$ and $k_m = 16$.

for $k_m = 6$ and $v = 0.2$ for $k_m = 2$. As seen in fig. 4 we observe an inverse energy transfer also for $v = 0.6$ contradicting the prediction made by [8]. This is probably due to the absence of any scaling regime for the configuration of forced and negative helical modes chosen here, as shown by panel (a) and (b) of fig. 4, and therefore our configuration does not satisfy the assumptions made in [8]. Figure 4(d) shows the balance of $\Pi_E(k)$ and $\mathrm{D}(k)$ for the wavenumbers $k \in [k_m, k_f]$ which confirms that negative helical modes lose energy due to molecular dissipation in such case.

Energy transfer for $k_m > k_f$

In this second set of simulations we forced at $k_f \in [4, 6]$ and kept the negative helical modes only for larger wavenumbers, $k_m = 10$ and $k_m = 16$. The behavior of the growth of energy is similar to the cases of $k_m < k_f$ (see fig. 5). After the negative helical modes become energetic they continue to accumulate energy and then reach a steady state by dissipating energy directly via molecular viscosity. However the dynamics of energy transfer

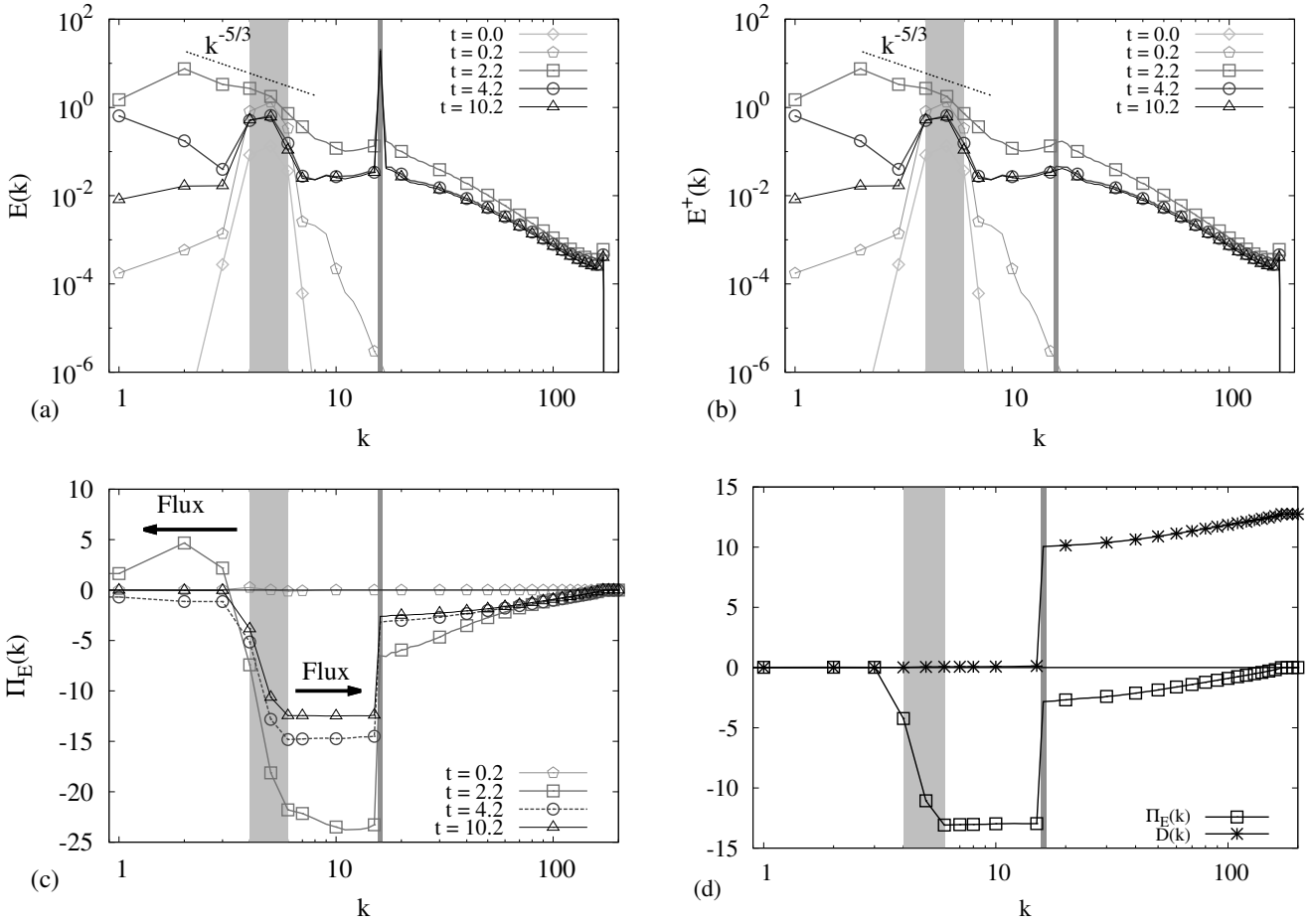

FIG. 6: The same of fig. 3 but for the case when $k_f \in [4, 6]$ and $k_m = 16$, except for (d) where energy flux and dissipation are compared at t 10 when the simulation is stopped (see fig. 5).

is entirely different from previous cases as seen in fig. 6. In fig. 6 (a) and (b) we show the spectrum for the total energy and for the positive helical modes respectively. As before, the difference between the two gives the energy content in the negative helical modes. In the beginning we initialize the field at the forced scales and we observe a clear inverse cascade of energy to large scales, shown by the energy spectra in fig. 6 (a) and (b) and in the positive energy flux in fig. 6(c) at $t \sim 2.2$. This transfer is due to the triads of Class I. Then, as soon as the negative helical modes become energetic enough, the triads of Class III and Class IV take the lead and the energy flux is reversed toward the negative helical modes at scales smaller than the forced ones from times $t \sim 4$ and larger. It is interesting to observe that the positive helical modes at large scales ($k < k_f$) also lose their energy by a forward cascade, probably highly nonlocal. Figure 6(c) shows the evolution of the energy flux during the backward and forward regimes. Panel (d) of the same figure compares the viscous contribution and the nonlinear flux. The figure shows that in the late stationary regime the viscous drag, induced by the high energy content of the negative helical modes, is balanced with the nonlinear flux. In this case we have a small-scales condensate that adsorbs all energy flowing between modes at $k \sim k_f$ and $k \sim k_m$. This is possibly due to the fact that positive helical modes at $k > k_m$ do not receive energy from the negative helical modes at $k \sim k_m$ as they could only form triads of Class II which are responsible for inverse energy transfer.

Coherent structures

As discussed in the previous sections, both experiments leads to a sort of helical condensate concentrated on the wavenumbers where the negative helical modes exists. This is a different way to produce (and stabilize) strong nonlinear structures in Navier-Stokes equations with respects to the well known case of two-dimensional turbulence [32–37]. A visualization of the vorticity field where an inverse cascade of energy is observed is shown in fig. 7(a). The presence of helical stable structures is clearly detectable. In panel (b) of the same figure we

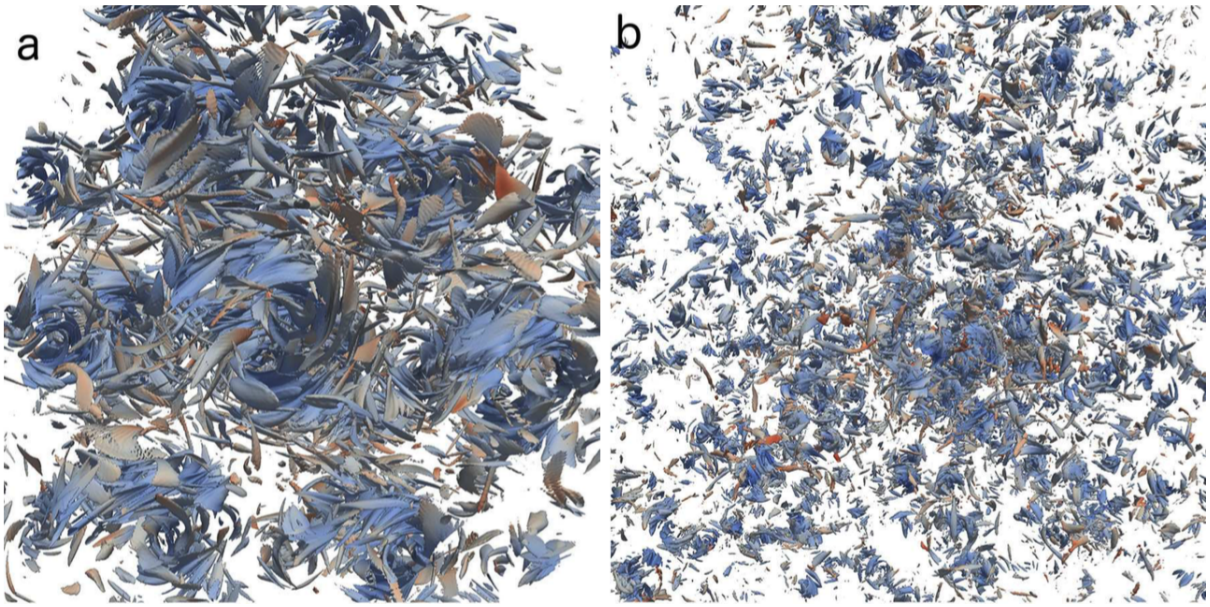

FIG. 7: (Color online) Iso-vorticity surfaces for: (a) $k_f = [10, 12]$, $k_m = 4$, (b) $k_f = [4 : 6]$, $k_m = 16$. Color palette is proportional to the intensity of the helicity: red for high positive values ($\sim 10^3$) to blue for high negative values ($\sim -10^3$).

show similar small-scales condensates that populate the flow when $k_f \in [4, 6]$ and $k_m = 16$. It would be interesting to understand if one can highlight some universality properties of such configurations as done for the two-dimensional case [37].

SUMMARY

We have performed several numerical simulations of a modified (decimated) version of the three-dimensional Navier-Stokes equations by keeping only some subsets of Fourier modes with different helical properties. The aim is to further understand the different roles played by triads with different helical structures in the dynamics of the nonlinear energy transfer mechanism. We have shown that as predicted in [8] there exist two classes (Class I and Class II) of triads that transfer energy to large scales, i.e. which can support an inverse cascade even in fully homogeneous and isotropic turbulence (but not mirror symmetric). This result for Class I where all modes have the same helical sign was already known [10, 25]. The second class (here called Class II) is made of triads where helicity is not globally sign-definite. The structure is such that the mode with the different helicity is the one at the smallest wavenumbers. Hence, when the small-scales are strongly helically-signed the forward energy transfer is depleted. The existence of inverse cascade even when helicity is not positive-definite contradicts the predictions based only on the absolute equilibrium in the inviscid and unforced limit [27, 28].
By concentrating the negative helical modes at small scales (high wavenumbers) we showed that as soon as triads of the other two classes (Class III and Class IV) become competitive, they take the leadership in the energy transfer mechanisms and the energy flux is reversed, reaching a more standard forward-cascade regime. In both cases the energy is preferentially transferred to the minority helical modes (here negative), leading to either a large-scale condensate or to a small-scales condensate. Our study further supports the idea that the direction of the energy transfer in a turbulent flow might strongly be influenced by the helicity distribution among different scales [10, 25, 26, 38, 39].

ACKNOWLEDGEMENT

We acknowledge useful discussions with F. Bonaccorso and funding from the European Research Council under the European Union Seventh Framework Programme, ERC Grant Agreement No 339032. Numerical simulations have been partially supported by the INFN initiative INF14_fldturb.

[1] A. N. Kolmogorov *Dokl. Akad. Nauk. SSSR* **32**, 19 (1941).
[2] U. Frisch, *Turbulence: the legacy of A.N. Kolmogorov* (Cambridge University Press, Cambridge, UK,1995).
[3] P. D. Mininni, A. Alexakis, and A. Pouquet, *Phys. Fluids* **21**, 015108 (2009).
[4] E. Deusebio and E. Lindborg, *J. Fluid Mech.* **755**, 654 (2014).

[5] A. Celani, S. Musacchio, and D. Vincenzi, *Phys. Rev. Lett.* **104**, 184506 (2010).
[6] A. Brandenburg, *Astrophysical J.* **550**, 824 (2001).
[7] U. Frisch, A. Pomyalov, I. Procaccia, and S. S. Ray *Phys. Rev. Lett.* **108**, 074501 (2012).
[8] F. Waleffe, *Phys Fluids A* **4**, 350 (1992).
[9] P. Constantin, A. Majda, *Commun. Math. Phys.* **115**, 435 (1988).
[10] L. Biferale, S. Musacchio, and F. Toschi, *J. Fluid Mech.* **730**, 309 (2013).
[11] L. Biferale and E. S. Titi, *J. Stat. Phys.* **151**, 1089 (2013).
[12] H. K. Moffatt, *J. Fluid Mech.* **35**, 117 (1969).
[13] H. K. Moffatt and A. Tsinober, *Annu. Rev. Fluid Mech.* **24**, 281 (1992).
[14] A. Brissaud, U. Frisch, J. Leorat, M. Lesieur, and M. Mazure, *Phys. Fluids* **16**, 1366 (1973).
[15] C.E. Laing, R. L. Ricca, and D. W. L. Summers, *Scientific Reports* **5**, 9224 (2015).
[16] P. D. Ditlevsen, *Phys. Fluids* **9**, 1482 (1997).
[17] D. D. Holm and R. M. Kerr, *Phys. Fluids* **19**, 025101 (2007).
[18] R. Benzi, L. Biferale, R. M. Kerr, and E. Trovatore, *Phys. Rev. E* **53**, 3541 (1996).
[19] Q. Chen, S. Chen, and G. L. Eyink, *Phys. Fluids* **15**, 361 (2003);
[20] Q. Chen, S. Chen, G. L. Eyink, and D. D. Holm, *Phys. Rev. Lett.* **90**, 214503 (2003).
[21] E. Herbert, F. Daviaud, B. Dubrulle, S. Nazarenko, and A. Naso, *Europhys. Lett.* **100**, 44003 (2012).
[22] D. Biskamp, *Magnetohydrodynamic Turbulence* (Cambridge University Press, Cambridge, UK, 2003).
[23] J. Baerenzung, H. Politano, Y. Ponty, and A. Pouquet, *Phys. Rev. E* **77**, 046303 (2008).
[24] P. D. Mininni and A. Pouquet, *Phys. Fluids* **22**, 035105 (2010).
[25] L. Biferale, S. Musacchio, and F. Toschi, *Phys. Rev. Lett.* **108**, 164501 (2012).
[26] G. Sahoo, F. Bonaccorsso, and L. Biferale, preprint, arXiv:1506.04906 (2015).
[27] C. Herbert, *Phys. Rev. E* **89**, 013010 (2014).
[28] R. H. Kraichnan, *J. Fluid Mech.* **47**, 525 (1971).
[29] K Seshasayanan, S. J. Benavides, and A. Alexakis, *Phys. Rev. E* **90**, 051003 (2014).
[30] K. Seshasayanan, A. Alexakis, preprint, arXiv:1509.02334 (2015).
[31] H. K. Moffatt, *J. Fluid Mech.* **741**, R3 (2014).
[32] R. H. Kraichnan, *Phys. Fluids* **10**, 1417 (1967).
[33] G. Boffetta and S. Musacchio, *Phys. Rev. E* **82**, 016307 (2010).
[34] M. Chertkov, C. Connaughton, I. Kolokolov, and V. Lebedev, *Phys. Rev. Lett.* **99**, 084501 (2007).
[35] M. Cencini, P. Muratore-Ginanneschi, and A. Vulpiani, *Phys. Rev. Lett.* **107**, 174502 (2011).
[36] H. J. H. Clercx, and G. J. F. van Heijst, *Appl. Mech. Rev.* **62**, 020802 (2009).
[37] J. Laurie, G. Boffetta, G. Falkovich, I. Kolokolov, and V. Lebedev, *Phys. Rev. Lett.* **113**, 254503 (2014).
[38] R. Stepanov, E. Golbraikh, P. Frick, and A. Shestakov, preprint, arXiv:1508.07236 (2015).
[39] M. Kessar, F. Plunian, R. Stepanov, and G. Balarac, preprint, arXiv:1509.02644 (2015).